

Measurement of the form factors of the decay $B^+ \rightarrow \bar{D}^{*0} \ell^+ \nu_\ell$ and determination of the CKM matrix element $|V_{cb}|$

I. Adachi,¹⁰ H. Aihara,⁵⁹ K. Arinstein,^{1,41} T. Aso,⁶³ V. Aulchenko,^{1,41} T. Aushev,^{26,19}
T. Aziz,⁵⁴ S. Bahinipati,³ A. M. Bakich,⁵³ V. Balagura,¹⁹ Y. Ban,⁴⁵ E. Barberio,³⁰
A. Bay,²⁶ I. Bedny,^{1,41} K. Belous,¹⁶ V. Bhardwaj,⁴⁴ B. Bhuyan,¹³ M. Bischofberger,³³
S. Blyth,³⁵ A. Bondar,^{1,41} A. Bozek,³⁷ M. Bračko,^{28,20} J. Brodzicka,³⁷ T. E. Browder,⁹
M.-C. Chang,⁴ P. Chang,³⁶ Y.-W. Chang,³⁶ Y. Chao,³⁶ A. Chen,³⁴ K.-F. Chen,³⁶
P.-Y. Chen,³⁶ B. G. Cheon,⁸ C.-C. Chiang,³⁶ R. Chistov,¹⁹ I.-S. Cho,⁶⁵ S.-K. Choi,⁷
Y. Choi,⁵² J. Crnkovic,¹² J. Dalseno,^{29,55} M. Danilov,¹⁹ A. Das,⁵⁴ M. Dash,⁶⁴
A. Drutskoy,³ W. Dungen,¹⁵ S. Eidelman,^{1,41} D. Epifanov,^{1,41} M. Feindt,²² H. Fujii,¹⁰
M. Fujikawa,³³ N. Gabyshev,^{1,41} A. Garmash,^{1,41} G. Gokhroo,⁵⁴ P. Goldenzweig,³
B. Golob,^{27,20} M. Grosse Perdekamp,^{12,47} H. Guo,⁴⁹ H. Ha,²³ J. Haba,¹⁰ B.-Y. Han,²³
K. Hara,³¹ T. Hara,¹⁰ Y. Hasegawa,⁵¹ N. C. Hastings,⁵⁹ K. Hayasaka,³¹ H. Hayashii,³³
M. Hazumi,¹⁰ D. Heffernan,⁴³ T. Higuchi,¹⁰ Y. Horii,⁵⁸ Y. Hoshi,⁵⁷ K. Hoshina,⁶²
W.-S. Hou,³⁶ Y. B. Hsiung,³⁶ H. J. Hyun,²⁵ Y. Igarashi,¹⁰ T. Iijima,³¹ K. Inami,³¹
A. Ishikawa,⁴⁸ H. Ishino,^{60,*} K. Itoh,⁵⁹ R. Itoh,¹⁰ M. Iwabuchi,⁶ M. Iwasaki,⁵⁹ Y. Iwasaki,¹⁰
T. Jinno,³¹ M. Jones,⁹ N. J. Joshi,⁵⁴ T. Julius,³⁰ D. H. Kah,²⁵ H. Kakuno,⁵⁹ J. H. Kang,⁶⁵
P. Kapusta,³⁷ S. U. Kataoka,³² N. Katayama,¹⁰ H. Kawai,² T. Kawasaki,³⁹ A. Kibayashi,¹⁰
H. Kichimi,¹⁰ C. Kiesling,²⁹ H. J. Kim,²⁵ H. O. Kim,²⁵ J. H. Kim,⁵² S. K. Kim,⁵⁰
Y. I. Kim,²⁵ Y. J. Kim,⁶ K. Kinoshita,³ B. R. Ko,²³ S. Korpar,^{28,20} M. Kreps,²²
P. Križan,^{27,20} P. Krokovny,¹⁰ T. Kuhr,²² R. Kumar,⁴⁴ T. Kumita,⁶¹ E. Kurihara,²
E. Kuroda,⁶¹ Y. Kuroki,⁴³ A. Kusaka,⁵⁹ A. Kuzmin,^{1,41} Y.-J. Kwon,⁶⁵ S.-H. Kyeong,⁶⁵
J. S. Lange,⁵ G. Leder,¹⁵ M. J. Lee,⁵⁰ S. E. Lee,⁵⁰ S.-H. Lee,²³ J. Li,⁹ A. Limosani,³⁰
S.-W. Lin,³⁶ C. Liu,⁴⁹ D. Liventsev,¹⁹ R. Louvot,²⁶ J. MacNaughton,¹⁰ F. Mandl,¹⁵
D. Marlow,⁴⁶ A. Matyja,³⁷ S. McOnie,⁵³ T. Medvedeva,¹⁹ Y. Mikami,⁵⁸ K. Miyabayashi,³³
H. Miyake,⁴³ H. Miyata,³⁹ Y. Miyazaki,³¹ R. Mizuk,¹⁹ A. Moll,^{29,55} T. Mori,³¹ T. Müller,²²
R. Mussa,¹⁸ T. Nagamine,⁵⁸ Y. Nagasaka,¹¹ Y. Nakahama,⁵⁹ I. Nakamura,¹⁰ E. Nakano,⁴²
M. Nakao,¹⁰ H. Nakayama,⁵⁹ H. Nakazawa,³⁴ Z. Natkaniec,³⁷ K. Neichi,⁵⁷ S. Neubauer,²²
S. Nishida,¹⁰ K. Nishimura,⁹ O. Nitoh,⁶² S. Noguchi,³³ T. Nozaki,¹⁰ A. Ogawa,⁴⁷
S. Ogawa,⁵⁶ T. Ohshima,³¹ S. Okuno,²¹ S. L. Olsen,⁵⁰ W. Ostrowicz,³⁷ H. Ozaki,¹⁰
P. Pakhlov,¹⁹ G. Pakhlova,¹⁹ H. Palka,³⁷ C. W. Park,⁵² H. Park,²⁵ H. K. Park,²⁵
K. S. Park,⁵² L. S. Peak,⁵³ M. Pernicka,¹⁵ R. Pestotnik,²⁰ M. Peters,⁹ L. E. Piilonen,⁶⁴
A. Poluektov,^{1,41} K. Prothmann,^{29,55} B. Riesert,²⁹ M. Rozanska,³⁷ H. Sahoo,⁹
K. Sakai,³⁹ Y. Sakai,¹⁰ N. Sasao,²⁴ O. Schneider,²⁶ P. Schönmeier,⁵⁸ J. Schümann,¹⁰
C. Schwanda,¹⁵ A. J. Schwartz,³ R. Seidl,⁴⁷ A. Sekiya,³³ K. Senyo,³¹ M. E. Sevier,³⁰
L. Shang,¹⁴ M. Shapkin,¹⁶ V. Shebalin,^{1,41} C. P. Shen,⁹ H. Shibuya,⁵⁶ S. Shiizuka,³¹
S. Shinomiya,⁴³ J.-G. Shiu,³⁶ B. Shwartz,^{1,41} F. Simon,^{29,55} J. B. Singh,⁴⁴ R. Sinha,¹⁷
A. Sokolov,¹⁶ E. Solovieva,¹⁹ S. Stanić,⁴⁰ M. Starić,²⁰ J. Stypula,³⁷ A. Sugiyama,⁴⁸
K. Sumisawa,¹⁰ T. Sumiyoshi,⁶¹ S. Suzuki,⁴⁸ S. Y. Suzuki,¹⁰ Y. Suzuki,³¹ F. Takasaki,¹⁰
N. Tamura,³⁹ K. Tanabe,⁵⁹ M. Tanaka,¹⁰ N. Taniguchi,¹⁰ G. N. Taylor,³⁰ Y. Teramoto,⁴²
I. Tikhomirov,¹⁹ K. Trabelsi,¹⁰ Y. F. Tse,³⁰ T. Tsuboyama,¹⁰ K. Tsunada,³¹ Y. Uchida,⁶
S. Uehara,¹⁰ Y. Ueki,⁶¹ K. Ueno,³⁶ T. Uglov,¹⁹ Y. Unno,⁸ S. Uno,¹⁰ P. Urquijo,³⁰
Y. Ushiroda,¹⁰ Y. Usov,^{1,41} G. Varner,⁹ K. E. Varvell,⁵³ K. Vervink,²⁶ A. Vinokurova,^{1,41}

C. C. Wang,³⁶ C. H. Wang,³⁵ J. Wang,⁴⁵ M.-Z. Wang,³⁶ P. Wang,¹⁴ X. L. Wang,¹⁴
M. Watanabe,³⁹ Y. Watanabe,²¹ R. Wedd,³⁰ J.-T. Wei,³⁶ J. Wicht,¹⁰ L. Widhalm,¹⁵
J. Wiechczynski,³⁷ E. Won,²³ B. D. Yabsley,⁵³ H. Yamamoto,⁵⁸ Y. Yamashita,³⁸
M. Yamauchi,¹⁰ C. Z. Yuan,¹⁴ Y. Yusa,⁶⁴ C. C. Zhang,¹⁴ L. M. Zhang,⁴⁹ Z. P. Zhang,⁴⁹
V. Zhilich,^{1, 41} V. Zhulanov,^{1, 41} T. Zivko,²⁰ A. Zupanc,²⁰ N. Zwahlen,²⁶ and O. Zyukova^{1, 41}

(The Belle Collaboration)

(The Belle Collaboration)

¹*Budker Institute of Nuclear Physics, Novosibirsk*

²*Chiba University, Chiba*

³*University of Cincinnati, Cincinnati, Ohio 45221*

⁴*Department of Physics, Fu Jen Catholic University, Taipei*

⁵*Justus-Liebig-Universität Gießen, Gießen*

⁶*The Graduate University for Advanced Studies, Hayama*

⁷*Gyeongang National University, Chinju*

⁸*Hanyang University, Seoul*

⁹*University of Hawaii, Honolulu, Hawaii 96822*

¹⁰*High Energy Accelerator Research Organization (KEK), Tsukuba*

¹¹*Hiroshima Institute of Technology, Hiroshima*

¹²*University of Illinois at Urbana-Champaign, Urbana, Illinois 61801*

¹³*India Institute of Technology Guwahati, Guwahati*

¹⁴*Institute of High Energy Physics,*

Chinese Academy of Sciences, Beijing

¹⁵*Institute of High Energy Physics, Vienna*

¹⁶*Institute of High Energy Physics, Protvino*

¹⁷*Institute of Mathematical Sciences, Chennai*

¹⁸*INFN - Sezione di Torino, Torino*

¹⁹*Institute for Theoretical and Experimental Physics, Moscow*

²⁰*J. Stefan Institute, Ljubljana*

²¹*Kanagawa University, Yokohama*

²²*Institut für Experimentelle Kernphysik, Universität Karlsruhe, Karlsruhe*

²³*Korea University, Seoul*

²⁴*Kyoto University, Kyoto*

²⁵*Kyungpook National University, Taegu*

²⁶*École Polytechnique Fédérale de Lausanne (EPFL), Lausanne*

²⁷*Faculty of Mathematics and Physics, University of Ljubljana, Ljubljana*

²⁸*University of Maribor, Maribor*

²⁹*Max-Planck-Institut für Physik, München*

³⁰*University of Melbourne, School of Physics, Victoria 3010*

³¹*Nagoya University, Nagoya*

³²*Nara University of Education, Nara*

³³*Nara Women's University, Nara*

³⁴*National Central University, Chung-li*

³⁵*National United University, Miao Li*

³⁶*Department of Physics, National Taiwan University, Taipei*

³⁷*H. Niewodniczanski Institute of Nuclear Physics, Krakow*

- ³⁸*Nippon Dental University, Niigata*
³⁹*Niigata University, Niigata*
⁴⁰*University of Nova Gorica, Nova Gorica*
⁴¹*Novosibirsk State University, Novosibirsk*
⁴²*Osaka City University, Osaka*
⁴³*Osaka University, Osaka*
⁴⁴*Panjab University, Chandigarh*
⁴⁵*Peking University, Beijing*
⁴⁶*Princeton University, Princeton, New Jersey 08544*
⁴⁷*RIKEN BNL Research Center, Upton, New York 11973*
⁴⁸*Saga University, Saga*
⁴⁹*University of Science and Technology of China, Hefei*
⁵⁰*Seoul National University, Seoul*
⁵¹*Shinshu University, Nagano*
⁵²*Sungkyunkwan University, Suwon*
⁵³*School of Physics, University of Sydney, NSW 2006*
⁵⁴*Tata Institute of Fundamental Research, Mumbai*
⁵⁵*Excellence Cluster Universe, Technische Universität München, Garching*
⁵⁶*Toho University, Funabashi*
⁵⁷*Tohoku Gakuin University, Tagajo*
⁵⁸*Tohoku University, Sendai*
⁵⁹*Department of Physics, University of Tokyo, Tokyo*
⁶⁰*Tokyo Institute of Technology, Tokyo*
⁶¹*Tokyo Metropolitan University, Tokyo*
⁶²*Tokyo University of Agriculture and Technology, Tokyo*
⁶³*Toyama National College of Maritime Technology, Toyama*
⁶⁴*IPNAS, Virginia Polytechnic Institute and State University, Blacksburg, Virginia 24061*
⁶⁵*Yonsei University, Seoul*

Abstract

We present a measurement of the Cabibbo-Kobayashi-Maskawa matrix element $|V_{cb}|$ times the form factor normalization $\mathcal{F}(1)$ using the decay $B^+ \rightarrow \bar{D}^{*0}\ell^+\nu_\ell$. This measurement is performed together with a determination of the form factor parameters ρ^2 , $R_1(1)$ and $R_2(1)$ which fully characterize this decay in the framework of Heavy Quark Effective Theory. This analysis is based on a data sample equivalent to 140 fb^{-1} of Belle data collected near the $\Upsilon(4S)$ resonance.

The preliminary results, based on about 27,000 reconstructed $B^+ \rightarrow \bar{D}^{*0}\ell^+\nu_\ell$ decays, are $\rho^2 = 1.376 \pm 0.074 \pm 0.056$, $R_1(1) = 1.620 \pm 0.091 \pm 0.092$, $R_2(1) = 0.805 \pm 0.064 \pm 0.036$ and $\mathcal{F}(1)|V_{cb}| = 35.0 \pm 0.4 \pm 2.2$. We find the $B^+ \rightarrow \bar{D}^{*0}\ell^+\nu_\ell$ branching fraction to be $(4.84 \pm 0.04 \pm 0.56)\%$. For all numbers quoted here, the first error is the statistical and the second is the systematic uncertainty.

A direct, model-independent determination of the form factor shapes has also been carried out and shows good agreement with the HQET based form factor parametrization by Caprini *et al.*.

*now at Okayama University, Okayama

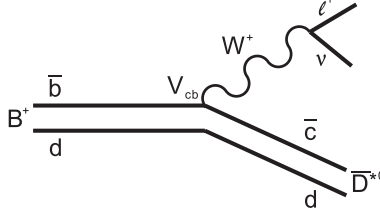


FIG. 1: Quark-level Feynman diagram for the decay $B^+ \rightarrow \bar{D}^{*0} \ell^+ \nu_\ell$.

I. INTRODUCTION

The magnitude of the Cabibbo-Kobayashi-Maskawa (CKM) matrix element $|V_{cb}|$ can be determined from exclusive decays $B \rightarrow \bar{D}^* \ell \nu$ [1]. In the framework of Heavy Quark Effective Theory (HQET), this decay is described by three form factor parameters, ρ^2 , $R_1(1)$ and $R_2(1)$ [2, 3] along with a form factor normalization $\mathcal{F}(1)$ derived from lattice QCD [4]. Many measurements of the B^0 mode are available which are unfortunately barely consistent [5], suggesting a hidden systematic uncertainty.

To shed light on this inconsistency, we now investigate the related decay $B^+ \rightarrow \bar{D}^{*0} \ell^+ \nu_\ell$ which carries different experimental systematics. This is interesting also because only few measurements of the B^+ mode are available in the literature [6, 7, 8].

This paper is organized as follows: after introducing the theoretical framework for the study of this decay, the experimental procedure is presented in detail. This is followed by a discussion of our results and the systematic uncertainties. Finally, a form factor parameterization independent measurement of the form factor shapes is described and results are given.

II. THEORETICAL FRAMEWORK

A. Kinematic variables

The decay $B^+ \rightarrow \bar{D}^{*0} \ell^+ \nu_\ell$ [9] proceeds chiefly through the tree-level transition shown in Fig. 1. Its kinematics can be fully characterized by four variables:

The first one is w , defined by

$$w = \frac{P_B \cdot P_{D^{*0}}}{m_B m_{D^{*0}}} = \frac{m_B^2 + m_{D^{*0}}^2 - q^2}{2m_B m_{D^{*0}}}, \quad (1)$$

where m_B and $m_{D^{*0}}$ are the masses of the B^+ and the D^{*0} mesons (5.2792 GeV/ c^2 and 2.007 GeV/ c^2 , respectively [10]), P_B and $P_{D^{*0}}$ are their four-momenta, and $q^2 = (P_\ell + P_\nu)^2$. In the B rest frame, approximately equal to the $\Upsilon(4S)$ center-of-mass (c.m.) frame, the expression for w reduces to the Lorentz boost $\gamma_{D^{*0}} = E_{D^{*0}}/m_{D^{*0}}$. The ranges of w and q^2 are restricted by the kinematics of the decay, with $q^2 = 0$ corresponding to

$$w_{\max} = \frac{m_B^2 + m_{D^{*0}}^2}{2m_B m_{D^{*0}}} \approx 1.505, \quad (2)$$

and $w_{\min} = 1$ to

$$q_{\max}^2 = (m_B - m_{D^{*0}})^2 \approx 10.71 \text{ GeV}^2/c^4. \quad (3)$$

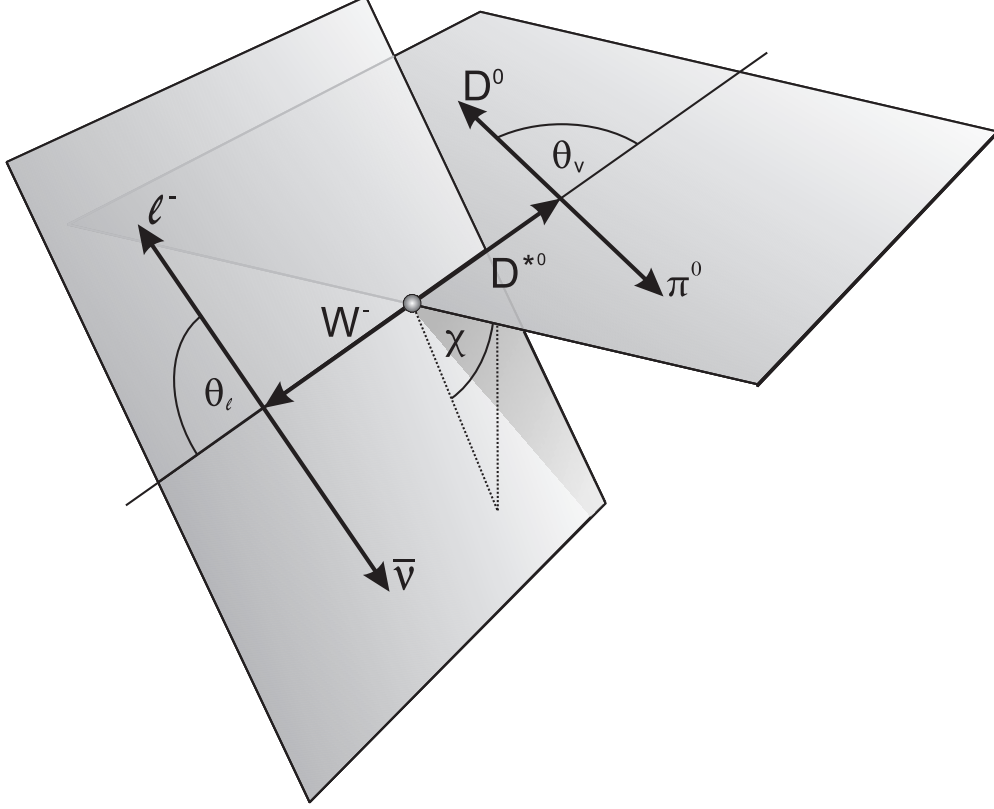


FIG. 2: Definition of the angles θ_ℓ , θ_V and χ for the decay $B^+ \rightarrow \bar{D}^{*0} \ell^+ \nu_\ell$, $D^{*0} \rightarrow D^0 \pi_s^0$.

The point $w = 1$ is also referred to as zero recoil.

The remaining three variables are the angles shown in Fig. 2:

- θ_ℓ , the angle between the direction of the lepton in the virtual W rest frame and the direction of the W in the B rest frame;
- θ_V , the angle between the direction of the D meson in the D^{*0} rest frame and the direction of the D^{*0} meson in the B rest frame;
- χ , the angle between the plane formed by the D^{*0} and the plane formed by the W decay.

B. Four-dimensional decay distribution

The Lorentz structure of the $B^+ \rightarrow \bar{D}^{*0} \ell^+ \nu_\ell$ decay amplitude can be expressed in terms of three helicity amplitudes (H_+ , H_- , and H_0), which correspond to the three polarization states of the D^{*0} , two transverse and one longitudinal. For low-mass leptons (electrons and muons), these amplitudes are expressed in terms of the three functions $h_{A_1}(w)$, $R_1(w)$, and $R_2(w)$ [2]

$$H_i(w) = m_B \frac{R^*(1-r^2)(w+1)}{2\sqrt{1-2wr+r^2}} h_{A_1}(w) \tilde{H}_i(w), \quad (4)$$

where

$$\tilde{H}_{\mp} = \frac{\sqrt{1-2wr+r^2} \left(1 \pm \sqrt{\frac{w-1}{w+1}} R_1(w)\right)}{1-r}, \quad (5)$$

$$\tilde{H}_0 = 1 + \frac{(w-1)(1-R_2(w))}{1-r}, \quad (6)$$

with $R^* = (2\sqrt{m_B m_{D^{*0}}})/(m_B + m_{D^{*0}})$ and $r = m_{D^{*0}}/m_B$. The functions $R_1(w)$ and $R_2(w)$ are defined in terms of the axial and vector form factors as,

$$A_2(w) = \frac{R_2(w)}{R^{*2}} \frac{2}{w+1} A_1(w), \quad (7)$$

$$V(w) = \frac{R_1(w)}{R^{*2}} \frac{2}{w+1} A_1(w). \quad (8)$$

By convention, the function $h_{A_1}(w)$ is defined as

$$h_{A_1}(w) = \frac{1}{R^*} \frac{2}{w+1} A_1(w). \quad (9)$$

For $w \rightarrow 1$, the axial form factor $A_1(w)$ dominates, and in the limit of infinite b - and c -quark masses, a single form factor describes the decay, the so-called Isgur-Wise function [11, 12].

The fully differential decay rate in terms of the three helicity amplitudes is

$$\begin{aligned} \frac{d^4\Gamma(B^+ \rightarrow \bar{D}^{*0}\ell^+\nu_\ell)}{dw d(\cos\theta_\ell) d(\cos\theta_V) d\chi} &= \frac{6m_B m_{D^{*0}}^2}{8(4\pi)^4} \sqrt{w^2-1} (1-2wr+r^2) G_F^2 |V_{cb}|^2 \\ &\times \left\{ (1-\cos\theta_\ell)^2 \sin^2\theta_V H_+^2(w) + (1+\cos\theta_\ell)^2 \sin^2\theta_V H_-^2(w) \right. \\ &+ 4\sin^2\theta_\ell \cos^2\theta_V H_0^2(w) - 2\sin^2\theta_\ell \sin^2\theta_V \cos 2\chi H_+(w) H_-(w) \\ &- 4\sin\theta_\ell (1-\cos\theta_\ell) \sin\theta_V \cos\theta_V \cos\chi H_+(w) H_0(w) \\ &\left. + 4\sin\theta_\ell (1+\cos\theta_\ell) \sin\theta_V \cos\theta_V \cos\chi H_-(w) H_0(w) \right\}, \end{aligned} \quad (10)$$

with $G_F = (1.16637 \pm 0.00001) \times 10^{-5} \text{ GeV}^{-2}$ [10]. By integrating this decay rate over all but one of the four variables, w , $\cos\theta_\ell$, $\cos\theta_V$, or χ , we obtain the four one-dimensional decay distributions from which we will extract the form factors. The differential decay rate as a function of w is

$$\frac{d\Gamma}{dw} = \frac{G_F^2}{48\pi^3} m_{D^{*0}}^3 (m_B - m_{D^{*0}})^2 \mathcal{G}(w) \mathcal{F}^2(w) |V_{cb}|^2, \quad (11)$$

where

$$\begin{aligned} \mathcal{F}^2(w) \mathcal{G}(w) &= h_{A_1}^2(w) \sqrt{w-1} (w+1)^2 \left\{ 2 \left[\frac{1-2wr+r^2}{(1-r)^2} \right] \right. \\ &\times \left[1 + R_1(w)^2 \frac{w-1}{w+1} \right] + \left[1 + (1-R_2(w)) \frac{w-1}{1-r} \right]^2 \left. \right\}, \end{aligned}$$

and $\mathcal{G}(w)$ is a known phase space factor,

$$\mathcal{G}(w) = \sqrt{w^2 - 1}(w + 1)^2 \left[1 + 4 \frac{w}{w + 1} \frac{1 - 2wr + r^2}{(1 - r)^2} \right].$$

In the infinite quark-mass limit, the heavy quark symmetry (HQS) predicts $\mathcal{F}(1) = 1$. Corrections to this limit have been calculated in lattice QCD. The most recent result obtained in unquenched lattice QCD reads $\mathcal{F}(1) = 0.921 \pm 0.013 \pm 0.020$ [4].

C. Form factor parameterization

The heavy quark effective theory (HQET) allows a parameterization of these form-factors to be obtained. Perfect heavy quark symmetry implies that $R_1(w) = R_2(w) = 1$, *i.e.*, the form factors A_2 and V are identical for all values of w and differ from A_1 only by a simple kinematic factor. Corrections to this approximation have been calculated in powers of Λ_{QCD}/m_b and the strong coupling constant α_s . Various parameterizations in powers of $(w - 1)$ have been proposed. Among the different predictions relating the coefficients of the higher order terms to the linear term, we adopt the following expressions derived by Caprini, Lellouch and Neubert [3],

$$h_{A_1}(w) = h_{A_1}(1) [1 - 8\rho^2 z + (53\rho^2 - 15)z^2 - (231\rho^2 - 91)z^3], \quad (12)$$

$$R_1(w) = R_1(1) - 0.12(w - 1) + 0.05(w - 1)^2, \quad (13)$$

$$R_2(w) = R_2(1) + 0.11(w - 1) - 0.06(w - 1)^2, \quad (14)$$

where $z = (\sqrt{w + 1} - \sqrt{2})/(\sqrt{w + 1} + \sqrt{2})$. The three parameters ρ^2 , $R_1(1)$, and $R_2(1)$, cannot be calculated; they must be extracted from data.

III. EXPERIMENTAL PROCEDURE

A. Data sample and event selection

The data used in this analysis were taken with the Belle detector [13] at the KEKB asymmetric energy e^+e^- collider [14]. Belle is a large-solid-angle magnetic spectrometer that consists of a silicon vertex detector (SVD), a 50-layer central drift chamber (CDC), an array of aerogel threshold Cherenkov counters (ACC), a barrel-like arrangement of time-of-flight scintillation counters (TOF), and an electromagnetic calorimeter (ECL) comprised of CsI(Tl) crystals located inside a super-conducting solenoid coil that provides a 1.5 T magnetic field. An iron flux-return located outside of the coil is instrumented to detect K_L^0 mesons and to identify muons (KLM). In the original setup the SVD was composed of three layers of double sided silicon strip modules, in 2003 it was upgraded and a fourth layer was added.

The data sample consists of 140 fb^{-1} taken at the $\Upsilon(4S)$ resonance, or 152×10^6 $B\bar{B}$ events. The entire data sample has been recorded using the three-layer SVD setup. Another 15 fb^{-1} taken at 60 MeV below the resonance are used to estimate the non- $B\bar{B}$ (continuum) background. The off-resonance data is scaled by the integrated on- to off-resonance luminosity ratio corrected for the $1/s$ dependence of the $q\bar{q}$ cross-section. This sample is identical to the one used for the $B^0 \rightarrow D^{*-} \ell^+ \nu_\ell$ analysis [15].

Monte Carlo (MC) samples equivalent to about three times the integrated luminosity are used in this analysis. MC simulated events are generated with the evtgen program [16] and full detector simulation based on GEANT [17] is applied. QED bremsstrahlung in $B \rightarrow X\ell\nu$ decays is added using the PHOTOS package [18].

Hadronic events are selected based on the charged track multiplicity and the visible energy in the calorimeter. The selection is described in detail elsewhere [19]. We also apply a moderate cut on the ratio of the second to the zeroth Fox-Wolfram moment [20], $R_2 < 0.4$, to reject continuum events.

B. Event reconstruction

Charged tracks are required to originate from the interaction point by applying the following selections on the impact parameters in $R\phi$ and z , $dr < 2$ cm and $|dz| < 4$ cm, respectively. Additionally, we demand at least one associated hit in the SVD detector. For pion and kaon candidates, the Cherenkov light yield from ACC, the time-of-flight information from TOF and dE/dx from CDC are required to be consistent with the respective mass hypothesis.

Neutral D meson candidates are searched for in the decays channels $D^0 \rightarrow K^-\pi^+$ and $D^0 \rightarrow K^-\pi^+\pi^-\pi^+$. We fit the charged tracks to a common vertex and reject the D^0 candidate if the χ^2 -probability is below 10^{-3} . The momenta of the charged tracks are re-evaluated at the vertex and the D^0 4-momentum is calculated as their sum. The reconstructed D^0 mass is required to lie within ± 3 standard deviations from the nominal mass [10], where one sigma (measured from real data) is about $4.5 \text{ MeV}/c^2$ ($4 \text{ MeV}/c^2$) for the one (three) pion mode.

The D^0 candidate is combined with a slow neutral pion π_s^0 to form a D^{*0} candidate. The π_s^0 is obtained by combining two photons with $E_\gamma > 100 \text{ MeV}$ for $\theta < 32^\circ$, $E_\gamma > 150 \text{ MeV}$ for $\theta > 130^\circ$, and $E_\gamma > 50 \text{ MeV}$ for photons detected in the barrel region. The invariant $\gamma\gamma$ mass has to lie within 3 standard deviations of the nominal π^0 mass, with $\sigma \approx 5 \text{ MeV}/c^2$. Additionally, a mass constraint fit is performed and the fit probability has to exceed 10^{-2} . Continuum suppression is achieved by requiring a D^{*0} momentum less than $2.45 \text{ GeV}/c$ in the c.m. frame.

Finally, the D^{*0} candidate is combined with a lepton (electron or muon), appropriately charged with respect to the kaon. Electron candidates are identified using the ratio of the energy detected in the ECL to the track momentum, the ECL shower shape, position matching between track and ECL cluster, the energy loss in the CDC and the response of the ACC counters. Muons are identified based on their penetration range and transverse scattering in the KLM detector. In the momentum region relevant to this analysis, charged leptons are identified with an efficiency of about 90% and the probability to misidentify a pion as an electron (muon) is 0.25% (1.4%) [21, 22]. No SVD hit requirement is made for lepton tracks. In the lab frame, the (transverse) momentum of the lepton is required to exceed $0.80 \text{ GeV}/c$ ($0.65 \text{ GeV}/c$) in case of electrons and $0.85 \text{ GeV}/c$ ($0.75 \text{ GeV}/c$) in case of muons. We also apply an upper lepton momentum cut at $2.4 \text{ GeV}/c$ in the c.m. frame to reject continuum.

In electron events, we attempt bremsstrahlung recovery by searching for photons in a cone of 3° around the electron track. If such a photon is found it is merged with the electron and the sum of the momenta is assumed to be the lepton momentum.

Figs. 3 and 4 show the invariant mass of the D^0 candidates and the π_s^0 momentum distributions, respectively.

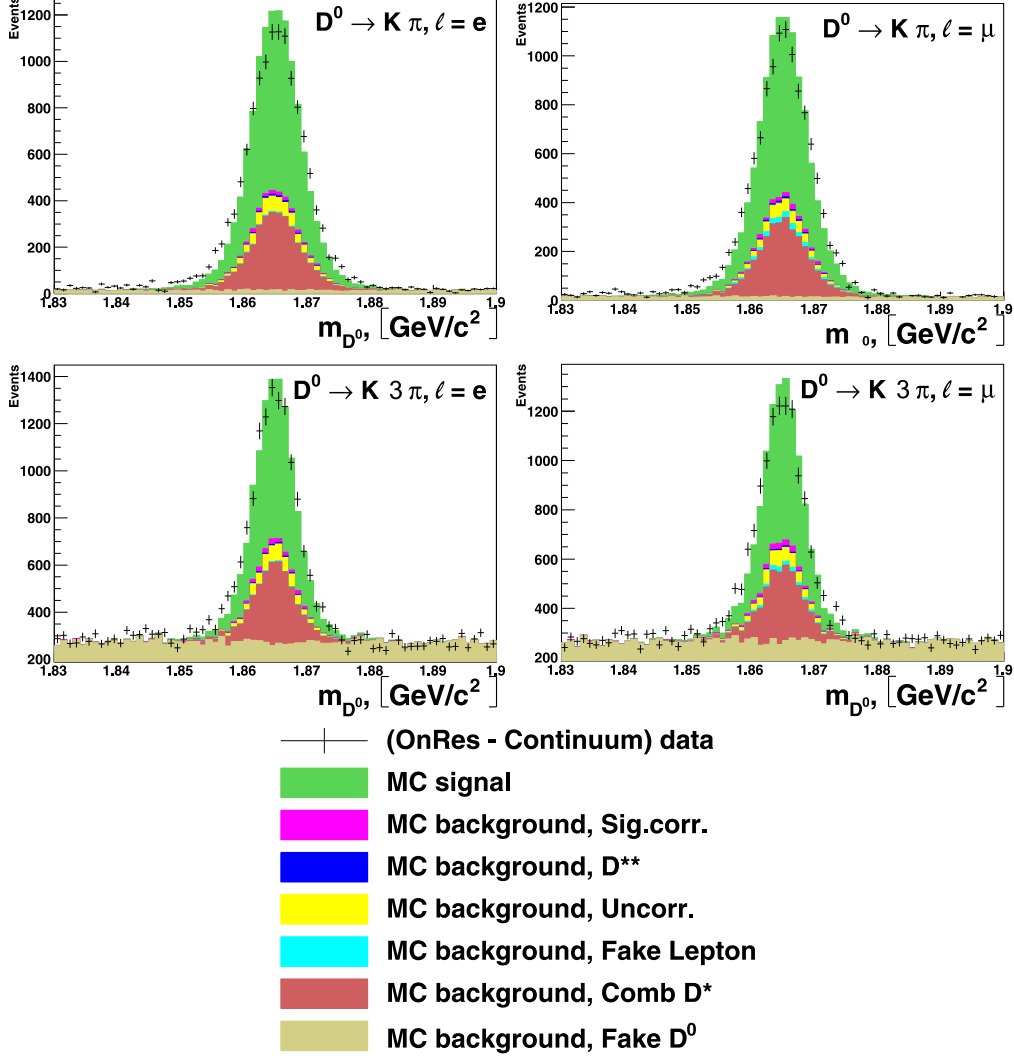


FIG. 3: Invariant D^0 candidate mass distributions in the different sub-samples. All analysis cuts (except on the plotted variable) are applied. The estimation of the background contributions is described in section III C.

C. Background estimation

Because we do not reconstruct the other B meson in the event, the B momentum is *a priori* unknown. However, in the c.m. frame, one can show that the B direction lies on a cone around the $(D^{*0}\ell)$ -axis [23],

$$\cos \theta_{B,D^{*0}\ell} = \frac{2E_B^* E_{D^{*0}\ell}^* - m_B^2 - m_{D^{*0}\ell}^2}{2|\vec{p}_B^*| |\vec{p}_{D^{*0}\ell}^*|}, \quad (15)$$

where E_B^* is half of the c.m. energy and $|\vec{p}_B^*|$ is $\sqrt{E_B^{*2} - m_B^2}$. The quantities $E_{D^{*0}\ell}^*$, $\vec{p}_{D^{*0}\ell}^*$ and $m_{D^{*0}\ell}$ are calculated from the reconstructed $D^{*0}\ell$ system.

This cosine is also a powerful discriminator between signal and background: signal events should strictly lie in the interval $(-1, 1)$, although – due to finite detector resolution – about

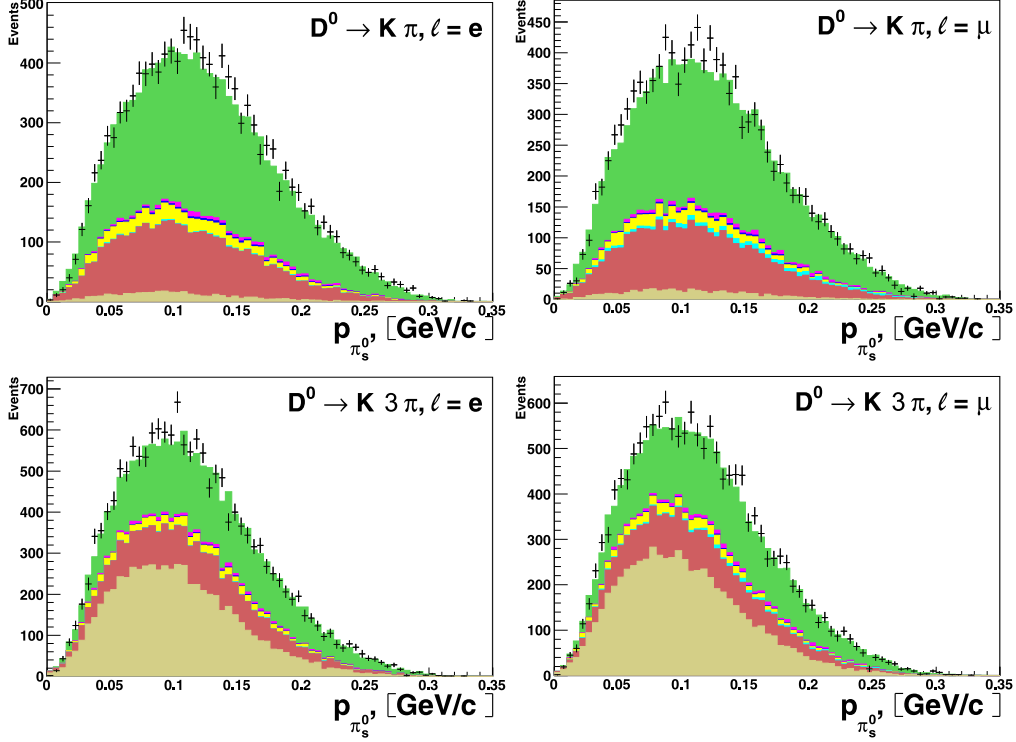


FIG. 4: Momentum distributions of the slow π^0 (lab frame) in the different sub-samples. All analysis cuts are applied. The color scheme is explained in Fig. 3. The estimation of the background contributions is described in section III C.

5% of the signal is reconstructed outside this interval. The background on the other hand does not have this restriction.

To determine the amount of signal and background in the selected events, we perform a two dimensional binned fit to $\cos\theta_{B,D^{*0}\ell}$ and Δm , the invariant mass difference between the D^{*0} and the D candidates. We consider backgrounds from the following six sources:

- continuum: any candidate reconstructed in a non- $\Upsilon(4S)$ event,
- fake D^0 : the D^0 candidate has been misreconstructed,
- combinatoric D^{*0} : the D^{*0} candidate is misreconstructed, however the D^0 candidate is identified correctly,
- fake lepton: the lepton has been misidentified but the D^{*0} is reconstructed properly,
- uncorrelated background: the D^{*0} and the lepton stem from different B mesons,
- D^{**} : background from $B \rightarrow \bar{D}^{**}\ell^+\nu$ decays with $\bar{D}^{**} \rightarrow \bar{D}^{*0}\pi$ or $B \rightarrow \bar{D}^{*0}\pi\ell^+\nu$ non-resonant, and
- correlated background: background from other processes in which the D^{*0} and the lepton stem from the same B meson, *e.g.* $B^+ \rightarrow \bar{D}^{*0}\tau^+\nu$, $\tau^+ \rightarrow \mu^+\nu\nu$.

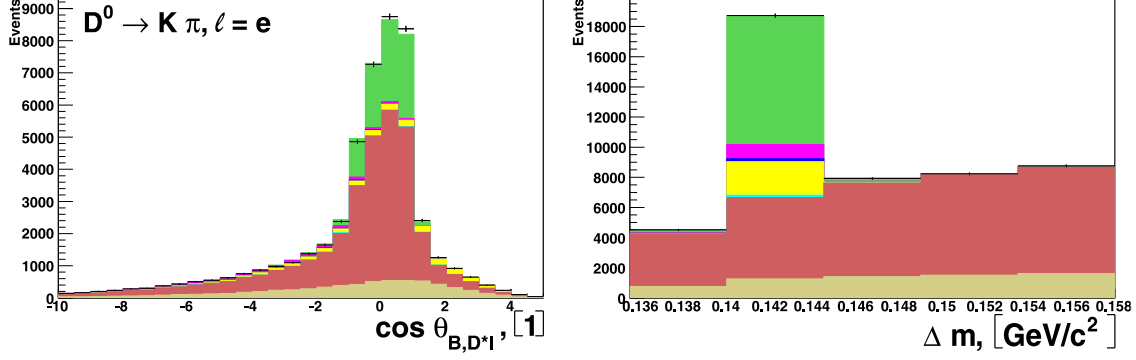


FIG. 5: Result of the fits to the $\cos \theta_{B,D^{*0}\ell}$ vs. Δm distributions in the $K\pi, e$ sub-sample. The projections in $\cos \theta_{B,D^{*0}\ell}$ and Δm are shown. The color scheme is explained in Fig. 3.

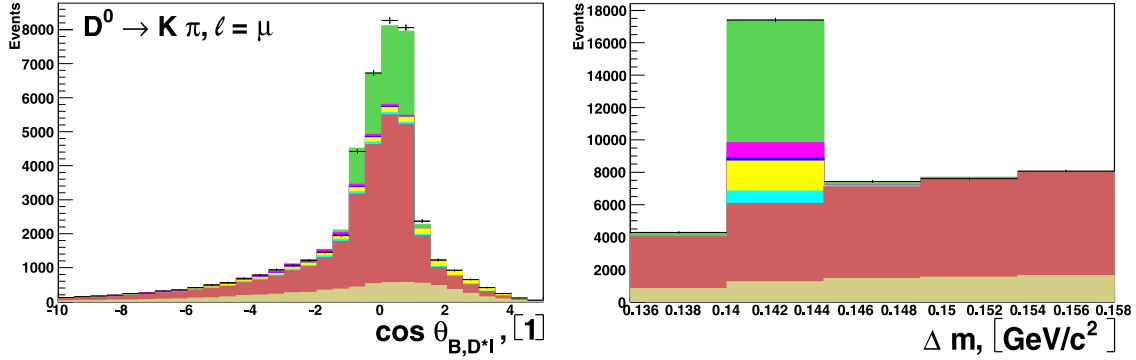


FIG. 6: Same of Fig. 5 for the $K\pi, \mu$ sub-sample.

These background components are modeled by MC ($D^{*0}\ell$) events, appropriately selected using generator information, except for continuum which is modeled by off-resonance events. For muon events, the shape of the fake lepton background is corrected by the ratio of the pion fake rate in the experimental data over the same quantity in the MC. The lepton identification efficiency is reweighted to compensate for imperfect MC simulation of the detector. The actual fit uses the `TFractionFitter` algorithm [24] in `ROOT` [25]. The fit is done separately in the four sub-samples defined by the D^0 decay channel and the lepton type. The results are shown in Figs. 5 to 8 and Table I.

In all fits, the continuum normalization is fixed to the on- to off-resonance luminosity ratio, corrected for the $1/s$ dependence of the $e^+e^- \rightarrow q\bar{q}$ cross-section. The on- to off-resonance luminosity ratio is measured using Bhabha events to an accuracy of 1.5 %. Aside from the before mentioned corrections to the lepton identification, the normalization of the fake lepton component has also been fixed to the MC expectations, since the fit failed to determine this small background contribution reliably. For the uncertainty in this component a very conservative value of 30% is assumed. The determination of the D^{**} and signal correlated backgrounds works reliably in the two $D^0 \rightarrow K^-\pi^+$ modes, but fails in the three pion channels. In these cases we fix the data to MC ratio to the value found in the former channels. We assume the relative uncertainty found in the $K\pi$ modes.

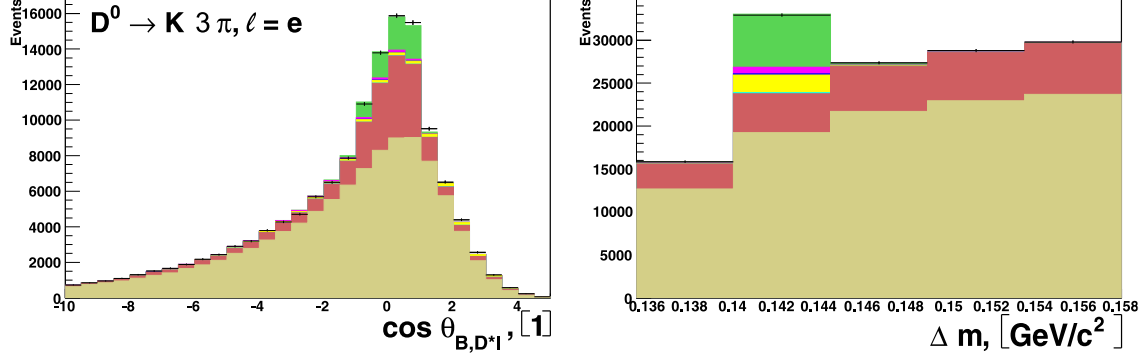


FIG. 7: Same of Fig. 5 for the $K3\pi, e$ sub-sample.

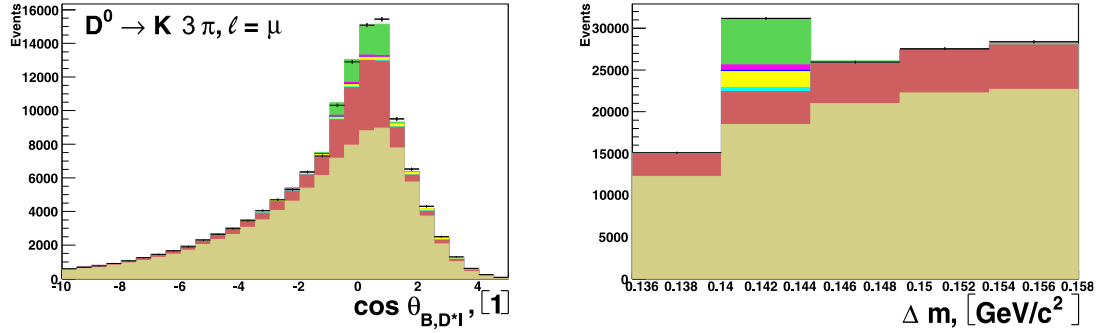


FIG. 8: Same of Fig. 5 for the $K3\pi, \mu$ sub-sample.

	$K\pi, e$	$K\pi, \mu$	$K3\pi, e$	$K3\pi, \mu$
Raw yield	13035	12262	16989	16350
Signal events	8133 ± 205	7447 ± 201	5987 ± 229	5539 ± 222
Signal	$(62.39 \pm 1.57)\%$	$(60.73 \pm 1.64)\%$	$(35.24 \pm 1.35)\%$	$(33.88 \pm 1.36)\%$
Signal correlated	$(1.27 \pm 0.31)\%$	$(1.46 \pm 0.32)\%$	$(1.16 \pm 0.26)\%$	$(1.34 \pm 0.31)\%$
D^{**}	$(0.77 \pm 0.98)\%$	$(0.73 \pm 0.98)\%$	$(0.39 \pm 0.50)\%$	$(0.36 \pm 0.47)\%$
Uncorrelated	$(4.97 \pm 0.54)\%$	$(4.25 \pm 0.45)\%$	$(3.48 \pm 0.41)\%$	$(3.30 \pm 0.38)\%$
Fake ℓ	$(0.31 \pm 0.10)\%$	$(1.94 \pm 0.59)\%$	$(0.18 \pm 0.06)\%$	$(0.95 \pm 0.29)\%$
Combinatoric D^{*0}	$(24.76 \pm 0.51)\%$	$(24.30 \pm 0.48)\%$	$(16.35 \pm 0.69)\%$	$(15.19 \pm 0.67)\%$
Fake D^0	$(2.91 \pm 0.25)\%$	$(3.12 \pm 0.23)\%$	$(38.53 \pm 0.50)\%$	$(39.45 \pm 0.51)\%$
Continuum	$(2.63 \pm 0.43)\%$	$(3.46 \pm 0.51)\%$	$(4.68 \pm 0.50)\%$	$(6.14 \pm 0.56)\%$

TABLE I: The signal and background fractions for selected events within the signal window $|\cos \theta_{B,D^{*0}\ell}| < 1$ and $140 \text{ MeV} < \Delta m < 144.5 \text{ MeV}$.

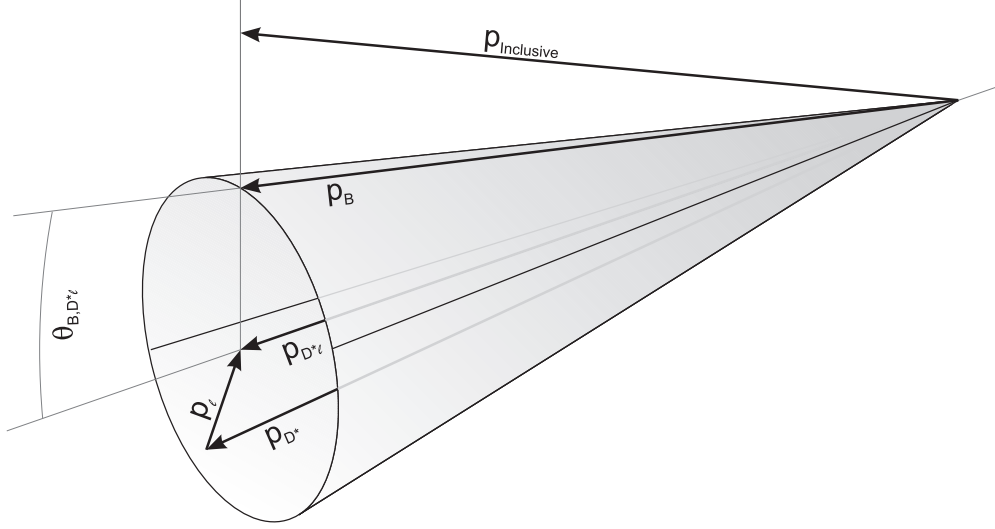


FIG. 9: Reconstruction of the B^+ direction. Refer to the text for details.

In Table I those components which have been fixed in the fit are shown with the corresponding error estimate described above. The error of the continuum component is appropriately scaled by the on- to off-resonance luminosity ratio.

In the rest of this analysis, we require $D^{*0}\ell$ candidates to pass the signal window requirement $-1 < \cos \theta_{B,D^{*0}\ell} < 1$ and $140 \text{ MeV} < \Delta m < 144.5 \text{ MeV}$.

D. Kinematic variables

To calculate the four kinematic variables – w , $\cos \theta_\ell$, $\cos \theta_V$ and χ – that characterize the $B^+ \rightarrow \bar{D}^{*0}\ell^+\nu$ decay defined in Sect. II A, we need to determine the B rest frame. The B direction is already known to be on a cone around the $(D^{*0}\ell)$ -axis with opening angle $2\theta_{B,D^{*0}\ell}$ in the c.m. frame, Eq. 15. For the best determination of the B direction, we first estimate the c.m. frame B vector by summing the momenta of the remaining particles in the event ($\vec{p}_{\text{inclusive}}^*$ [23]) and choose the direction on the cone that minimizes the difference to $\vec{p}_{\text{inclusive}}^*$, Fig. 9.

To obtain $\vec{p}_{\text{inclusive}}^*$, we first apply the following track and cluster selection requirements to particles which have not been associated with the $(D^{*0}\ell)$ system: neutral clusters are required to satisfy $E_\gamma > 100 \text{ MeV}$ for polar angles with respect to the beam direction $\theta < 32^\circ$, $E_\gamma > 150 \text{ MeV}$ for $\theta > 130^\circ$ and $E_\gamma > 50 \text{ MeV}$ in the barrel region in between; the impact parameter cuts for charged tracks are $dr < 20 \text{ cm}$ and $|dz| < 100 \text{ cm}$ for $p_T < 0.25 \text{ GeV}/c$, $dr < 15 \text{ cm}$ and $|dz| < 50 \text{ cm}$ for $p_T < 0.5 \text{ GeV}/c$, and $dr < 10 \text{ cm}$ and $|dz| < 20 \text{ cm}$ for $p_T > 0.5 \text{ GeV}/c$. We exclude duplicated tracks by selecting pairs of charged tracks with $p_T < 275 \text{ MeV}/c$, momentum difference $\Delta p < 100 \text{ MeV}/c$ and relative angle smaller than 15° or larger than 165° . If such a pair is found, only the track with smaller value of $(5 dr)^2 + (|dz|)^2$ is retained.

Then, we compute $\vec{p}_{\text{inclusive}}$ (in the lab. frame) by summing the 3-momenta of the selected

particles,

$$\vec{p}_{\text{inclusive}} = \vec{p}_{\text{HER}} + \vec{p}_{\text{LER}} - \sum_i \vec{p}_i, \quad (16)$$

where the indices HER and LER correspond to the colliding beams, and transform this vector into the c.m. frame. Note that we do not make any mass assumption for the charged particles. The energy component of the 4-vector $P_{\text{inclusive}}$ is defined by requiring $E_{\text{inclusive}}^*$ to be $E_{\text{beam}}^* = \sqrt{s}/2$.

With the B rest frame reconstructed in this way, the resolutions in the kinematic variables are found to be about 0.021, 0.049, 0.057 and 6.46° for w , $\cos\theta_\ell$, $\cos\theta_V$ and χ , respectively.

E. Fit procedure

We perform a binned χ^2 fit of the w , $\cos\theta_\ell$, $\cos\theta_V$ and χ distributions over (almost) the entire phase space to measure the following quantities: the form factor normalization $\mathcal{F}(1)|V_{cb}|$, Eq. 11, and the three parameters ρ^2 , $R_1(1)$ and $R_2(1)$ which parameterize the form factor in the HQET framework, Eqs. 12–14. Instead of fitting in four dimensions, we fit the one-dimensional projections of w , $\cos\theta_\ell$, $\cos\theta_V$ and χ to have enough entries in each bin of the fit. This introduces bin-to-bin correlations which have to be accounted for.

The distributions in w , $\cos\theta_\ell$, $\cos\theta_V$ and χ are divided into ten bins of equal width. The kinematically allowed values of w are between 1 and ≈ 1.505 but we restrict the w range to values between 1 and 1.5. In each sub-sample, there are thus 40 bins to be used in the fit. In the following, we label these bins with a common index i , $i = 1, \dots, 40$. The bins $i = 1, \dots, 10$ correspond to the bins of the w distribution, $i = 11, \dots, 20$ to $\cos\theta_\ell$, $i = 21, \dots, 30$ to $\cos\theta_V$ and $i = 31, \dots, 40$ to the χ distribution.

The predicted number of events N_i^{th} in the bin i is given by

$$N_i^{\text{th}} = N_{B^+} \mathcal{B}(D^{*0} \rightarrow D^0 \pi^0) \mathcal{B}(D^0) \tau_{B^+} \Gamma_i, \quad (17)$$

where N_{B^+} is the number of B^+ mesons in the data sample and $\mathcal{B}(D^{*0} \rightarrow D^0 \pi^0)$ is taken from Ref. [10]. In the $(K\pi, e)$ and $(K\pi, \mu)$ sub-samples $\mathcal{B}(D^0)$ is $\mathcal{B}(D^0 \rightarrow K^- \pi^+)$ [10]; in $(K3\pi, e)$ and $(K3\pi, \mu)$ $\mathcal{B}(D^0)$ is $R_{K3\pi/K\pi} \mathcal{B}(D^0 \rightarrow K^- \pi^+)$, with $R_{K3\pi/K\pi}$ a fifth free parameter of the fit. Finally, τ_{B^+} is the B^+ lifetime [10], and Γ_i is the width obtained by integrating Eq. 10 in the kinematic variable corresponding to i from the lower to the upper bin boundary (the other kinematic variables are integrated over their full range). This integration is numerical in the case of w and analytic for the other variables. The expected number of events N_i^{exp} is related to N_i^{th} as follows

$$N_i^{\text{exp}} = \sum_{j=1}^{40} (R_{ij} \epsilon_j N_j^{\text{th}}) + N_i^{\text{bkgrd}}. \quad (18)$$

Here, ϵ_i is the probability that an event generated in the bin i is reconstructed and passes all analysis cuts and R_{ij} is the detector response matrix, *i.e.*, it gives the probability that an event generated in the bin j is observed in the bin i . Both quantities are calculated using MC simulation. N_i^{bkgrd} is the number of expected background events, estimated as described in Sect. III C.

Next, we calculate the variance σ_i^2 of N_i^{exp} . We consider the following contributions: the poissonian uncertainty in N_i^{th} ; fluctuations related to the efficiency, which are investigated

using a binomial distribution with N repetitions and the success probability ϵ_i ; a similar contribution based on a multinomial distribution related to R_{ij} ; and the uncertainty in the background contribution N_i^{bkgrd} . This yields the following expression for σ_i^2 ,

$$\sigma_i^2 = \sum_{j=1}^{40} \left[R_{ij}^2 \epsilon_j^2 N_j^{\text{th}} + R_{ij}^2 \frac{\epsilon_j(1-\epsilon_j)}{N_{\text{data}}} (N_j^{\text{th}})^2 + \frac{R_{ij}(1-R_{ij})}{N'_{\text{data}}} \epsilon_j^2 (N_j^{\text{th}})^2 + \right. \\ \left. R_{ij}^2 \frac{\epsilon_j(1-\epsilon_j)}{N_{\text{MC}}} (N_j^{\text{th}})^2 + \frac{R_{ij}(1-R_{ij})}{N'_{\text{MC}}} \epsilon_j^2 (N_j^{\text{th}})^2 \right] + \sigma^2(N_i^{\text{bkgrd}}). \quad (19)$$

The first term is the poissonian uncertainty in N_i^{th} . The second and third terms are the binomial respectively multinomial uncertainties related to the finite real data size, where N_{data} (N'_{data}) is the total number of decays (the number of reconstructed decays) into the final state under consideration ($K\pi$ or $K3\pi$, e or μ) in the real data. The quantities ϵ_i and R_{ij} are calculated from a finite signal MC sample (N_{MC} and N'_{MC}); the corresponding uncertainties are estimated by the fourth and fifth terms. Finally, the last term is the background contribution $\sigma^2(N_i^{\text{bkgrd}})$, calculated as the sum of the different background component variances. For each background component defined in Sect. III C we estimate its contribution by linear error propagation of the scale factor and the error determined by the procedure described above.

In each sub-sample we calculate the off-diagonal elements of the covariance matrix cov_{ij} as $Np_{ij} - Np_i p_j$, where p_{ij} is the relative abundance of the bin (i, j) in the 2-dimensional histogram obtained by plotting the kinematic variables against each other, p_i is the relative number of entries in the 1-dimensional distribution, and N is the size of the sample. Covariances are calculated for the signal and the different background components, and added with appropriate normalizations.

The covariance matrix is inverted numerically within ROOT and, labelling the four sub-samples ($K\pi$ or $K3\pi$, e or μ) with the index k , the sub-sample χ^2 functions are calculated,

$$\chi_k^2 = \sum_{i,j} (N_i^{\text{obs}} - N_i^{\text{exp}}) C_{ij}^{-1} (N_j^{\text{obs}} - N_j^{\text{exp}}), \quad (20)$$

where N_i^{obs} is the number of events observed in bin i in the data. We sum these four functions and minimize the global χ^2 with MINUIT [26].

We have tested this fit procedure for possible biases using MC samples, generated both with and without full detector simulation. All results are consistent with expectations and show no indication of bias.

IV. RESULTS AND SYSTEMATIC UNCERTAINTIES

A. Results

After applying all analysis cuts and subtracting backgrounds, $27,106 \pm 367$ signal events are found in the data. The preliminary result of the fit to these events is shown in Fig. 10 and Tab. II. The correlation coefficients of the five fit parameters are given in Tab. III. The breakup of the systematic uncertainty is given in Tab. IV.

As explained earlier, the branching fraction of the decay $D^0 \rightarrow K^- \pi^+ \pi^+ \pi^-$ is floated in the fit to the full sample. The fit result is in good agreement with the world average [10]. In the sub-sample fits, $R_{K3\pi/K\pi}$ is fixed to the value of the full sample fit.

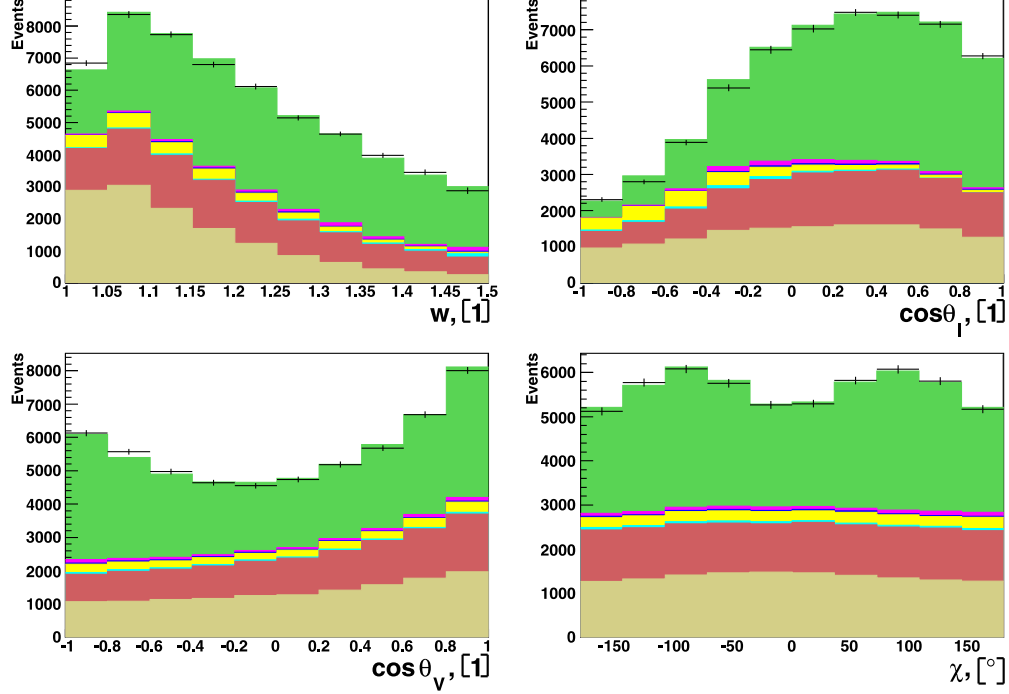


FIG. 10: Result of the fit of the four kinematic variables in the total sample. (The different sub-samples are added in this plot.) The points with error bars are continuum subtracted on-resonance data. The histograms are the signal and the different background components. The color scheme is explained in Fig. 3.

B. Systematic uncertainties

To estimate the systematic errors in the results quoted above, we consider uncertainties in the following: signal reconstruction efficiency, background estimation, $D^{*0} \rightarrow D^0 \pi^0$ and $D^0 \rightarrow K^- \pi^+$ branching fractions [10], B^+ lifetime [10], and the number of B^+ mesons in the data sample.

To calculate these systematic uncertainties, we consider 300 pseudo-experiments in which 13 quantities (corresponding to the above-mentioned contributions) are randomly varied, taking into account possible correlations. The entire analysis chain is repeated for every pseudo-experiment and new fit values are obtained. One standard deviation of the pseudo-experiment fit results for a given parameter is used as the systematic uncertainty in this parameter. This toy MC approach also allows the systematic correlation coefficients in Table III to be derived in a straightforward way.

In the following, we describe the parameters varied in the pseudo-experiments:

- The tracking efficiencies in five bins of slow pion momentum are varied within their respective uncertainties. These uncertainties are determined from real data by studying the decay $B^+ \rightarrow \bar{D}^{*0} \pi^+$ in the same 140 fb^{-1} sample as used for the main analysis. The tracking uncertainties in different momentum bins are considered fully correlated. Therefore, tracking corresponds only to a single parameter in the toy MC,
- The lepton identification uncertainties are varied within their respective uncertain-

	$D^0 \rightarrow K\pi. \ell = e$	$D^0 \rightarrow K\pi. \ell = \mu$	$D^0 \rightarrow K3\pi. \ell = e$
ρ^2	$1.199 \pm 0.125 \pm 0.048$	$1.370 \pm 0.129 \pm 0.057$	$1.723 \pm 0.162 \pm 0.061$
$R_1(1)$	$1.507 \pm 0.135 \pm 0.090$	$1.568 \pm 0.158 \pm 0.088$	$1.840 \pm 0.271 \pm 0.109$
$R_2(1)$	$0.868 \pm 0.093 \pm 0.034$	$0.839 \pm 0.110 \pm 0.031$	$0.585 \pm 0.198 \pm 0.047$
$R_{K3\pi/K\pi}$	2.072	2.072	2.072
$\mathcal{B}(B^+ \rightarrow \bar{D}^{*0} \ell^+ \nu_\ell)$	$4.91 \pm 0.05 \pm 0.57$	$4.77 \pm 0.05 \pm 0.56$	$4.83 \pm 0.07 \pm 0.56$
$\mathcal{F}(1) V_{cb} \times 10^3$	$34.3 \pm 0.6 \pm 2.2$	$35.0 \pm 0.6 \pm 2.3$	$36.5 \pm 1.0 \pm 2.3$
$\chi^2/\text{ndf.}$	48.3 / 36	40.6 / 36	39.6 / 36
P_{χ^2}	8.3 %	27.5 %	31.3 %

	$D^0 \rightarrow K3\pi. \ell = \mu$	Fit to total sample
ρ^2	$1.434 \pm 0.209 \pm 0.086$	$1.376 \pm 0.074 \pm 0.056$
$R_1(1)$	$1.813 \pm 0.273 \pm 0.106$	$1.620 \pm 0.091 \pm 0.092$
$R_2(1)$	$0.764 \pm 0.191 \pm 0.051$	$0.805 \pm 0.064 \pm 0.036$
$R_{K3\pi/K\pi}$	2.072	2.072 ± 0.023
$\mathcal{B}(B^+ \rightarrow \bar{D}^{*0} \ell^+ \nu_\ell)$	$4.83 \pm 0.07 \pm 0.57$	$4.84 \pm 0.04 \pm 0.56$
$\mathcal{F}(1) V_{cb} \times 10^3$	$34.8 \pm 1.0 \pm 2.3$	$35.0 \pm 0.4 \pm 2.2$
$\chi^2/\text{ndf.}$	44.2 / 36	187.8 / 155
P_{χ^2}	16.3 %	3.7 %

TABLE II: The results of the fits to the sub-samples and to the total sample. The first error is statistical, the second is the estimated systematic uncertainty.

	$\mathcal{F}(1) V_{cb} $	ρ^2	$R_1(1)$	$R_2(1)$
$\mathcal{F}(1) V_{cb} $	1.000	0.455/0.399/0.295	-0.222 / -0.219 / -0.179	-0.054 / -0.024 / -0.019
ρ^2		1.000	0.648 / 0.413 / 0.540	-0.889 / -0.751 / -0.841
$R_1(1)$			1.000	-0.749 / -0.873 / -0.763
$R_2(1)$				1.000

TABLE III: The statistical/systematic/total correlation coefficients for $\mathcal{F}(1)|V_{cb}|$ and the three form factor parameters in the fit to the full sample.

ties [21, 22],

- The normalizations of the 7 background components are varied within the uncertainties determined by the background fit in Sect. III C. For continuum, the on- to off-resonance luminosity ratio is varied within its uncertainty of 1.5%. Correlations between different background component normalizations are taken into account,
- Additionally, we vary the shape in w of the uncorrelated, combinatoric D^{*0} and fake D^0 components. We fit each of these distributions by a Lorentz distribution and vary each of the parameters within the errors obtained in the fit,

	ρ^2	$R_1(1)$	$R_2(1)$	$\mathcal{F}(1) V_{cb} \times 10^3$	$\mathcal{B}(B^+ \rightarrow \bar{D}^{*0}\ell^+\nu_\ell)$
Value	1.376	1.620	0.805	34.98	4.841
Statistical Error	0.074	0.091	0.064	0.37	0.044
Tracking	-0.027	+0.025	+0.012	-1.97	-0.491
LeptonID	+0.012	+0.024	-0.011	-0.39	-0.096
Norm - Signal Corr.	-0.007	+0.002	+0.007	+0.13	+0.038
Norm - D^{**}	+0.005	-0.023	+0.002	-0.04	-0.041
Norm - Uncorr	+0.014	+0.074	-0.025	-0.28	-0.023
Norm - Fake ℓ	+0.017	+0.028	-0.010	-0.05	-0.024
Norm - Comb D^{*0}	+0.008	+0.014	-0.008	-0.11	-0.028
Norm - Fake D^0	-0.009	-0.014	+0.007	+0.06	+0.020
Norm - Continuum	+0.004	+0.005	-0.001	0.00	-0.003
Shape - Uncorr	+0.014	+0.003	-0.005	+0.10	
Shape - Comb D^{*0}	+0.027	-0.005	-0.008	+0.21	
Shape - Fake D^0	+0.024	+0.003	+0.008	+0.17	
$\mathcal{B}(D^0 \rightarrow K\pi)$				-0.32	-0.089
$\mathcal{B}(D^{*0} \rightarrow D^0\pi^0)$				-0.82	-0.227
B^+ lifetime				-0.12	-0.033
$N(\Upsilon(4S))$				-0.14	-0.040
f_{+-}/f_{00}	+0.003	+0.006	-0.003	-0.15	-0.043

TABLE IV: The breakup of the systematic uncertainty in the result of the fit to the full sample. The sign + (-) implies whether the fit result moves to larger (smaller) values, if the value of the corresponding systematic parameter is increased.

- We vary the fraction $f_{+-}/f_{00} = \mathcal{B}(\Upsilon(4S) \rightarrow B^+B^-)/\mathcal{B}(\Upsilon(4S) \rightarrow B^0\bar{B}^0)$ within its uncertainty [10]. This parameter affects the background distributions.

The uncertainties in $\mathcal{B}(D^{*0} \rightarrow D^0\pi^0)$, $\mathcal{B}(D^0 \rightarrow K^-\pi^+)$, the number of B^+ in the sample and the B^+ lifetime affect only $\mathcal{F}(1)|V_{cb}|$, not the form factors. Therefore, they are not considered in the toy MC.

The breakup of the systematic errors quoted in Table II is given in Table IV.

V. MODEL-INDEPENDENT DETERMINATION OF HELICITY AMPLITUDES

The results discussed in the previous section rely on the form factor parameterization by Caprini *et al.* [3] and it is worthwhile to check this assumption. In this section, we extract the form factor shape through a fit to the w vs. $\cos\theta_V$ distribution. For the former quantity, we consider six bins in the range from 1 to 1.5. For the latter, we have also six bins between -1 and 1 . The contribution from events with $w > 1.5$ is fixed to the very small values predicted by the results of the parametrized fit.

A. Fit procedure

From Eq. 10 we can obtain the double differential decay width $d^2\Gamma/dw d\cos\theta_V$ by integration over $\cos\theta_\ell$ and χ .

If we define

$$F_\Gamma = \frac{3 G_F^2 (m_B - m_{D^*})^2 m_{D^*}^3}{4^5 \pi^4} \quad (21)$$

and

$$\begin{aligned} \gamma^{\pm\pm}(w) &= \sqrt{w^2 - 1} (w + 1)^2 h_{A_1}^2(w) |V_{cb}|^2 \frac{1 - 2wr - r^2}{(1 - r)^2} \left\{ 1 \mp \sqrt{\frac{w - 1}{w + 1}} R_1(w) \right\}^2, \\ \gamma^{00}(w) &= \sqrt{w^2 - 1} (w + 1)^2 h_{A_1}^2(w) |V_{cb}|^2 \left\{ 1 + \frac{w - 1}{1 - r} (1 - R_2(w)) \right\}^2, \end{aligned} \quad (22)$$

the double differential width becomes

$$\frac{d^2\Gamma(B^+ \rightarrow \bar{D}^{*0} \ell^+ \nu_\ell)}{dw d(\cos\theta_V)} = \frac{16\pi}{3} F_\Gamma (\sin^2\theta_V (\gamma^{++} + \gamma^{--}) + 2 \cos^2\theta_V \gamma^{00}). \quad (23)$$

The quantities γ^{kk} correspond to the w -dependence of the different helicity combinations, times kinematic factors. The one dimensional distribution, as given in Eq. 11, depends only on the sum of these three combinations,

$$\frac{d\Gamma(B^+ \rightarrow \bar{D}^{*0} \ell^+ \nu_\ell)}{dw} = \frac{64\pi}{9} F_\Gamma (\gamma^{++} + \gamma^{--} + \gamma^{00}). \quad (24)$$

The bin contents of the two dimensional histogram in w vs. $\cos\theta_V$ can be obtained by integration of Eq. 23 over the corresponding bin area and considering the reconstruction efficiencies and detector response as described in Eq. 18. Each bin content can be given as the linear combination of two linearly independent parts. The integration of the angular distributions is executed analytically, as described in Sect. III E, the integration with respect to w defines a set of free parameters,

$$\Gamma_i^{kk} = \int_{w_i}^{w_{i+1}} dw \gamma^{kk}, \quad (25)$$

where $w_j = \{w_1, w_2, \dots, w_7\} = \{1, 13/12, \dots, 1.5\}$ are the bin boundaries of the 6 bins in w . Additionally we define $\gamma^T = \gamma^{++} + \gamma^{--}$ and $\Gamma_i^T = \Gamma_i^{++} + \Gamma_i^{--}$.

We define the χ^2 function $\tilde{\chi}_{w,\theta_V}^2 = \sum_{i=1}^6 \sum_{j=1}^6 \left(\frac{N_{ij}^{obs} - N_{ij}^{exp}}{\sigma_{N^{exp}}} \right)^2$, which depends only on the parameters Γ_i^T and Γ_i^{00} . Here N_{ij}^{obs} gives the number of events observed in on-resonance data, N_{ij}^{exp} the number of expected events, as defined in Eq. 18, and $\sigma_{N^{exp}}$ the uncertainty in the expected number of events, as given in Eq. 19. This expression is minimized numerically using MINUIT to determine the partial integrals.

Investigation of dedicated sets of toy Monte Carlo showed the reliability of the procedure described above. The results show no indication of bias in either the mean or the errors.

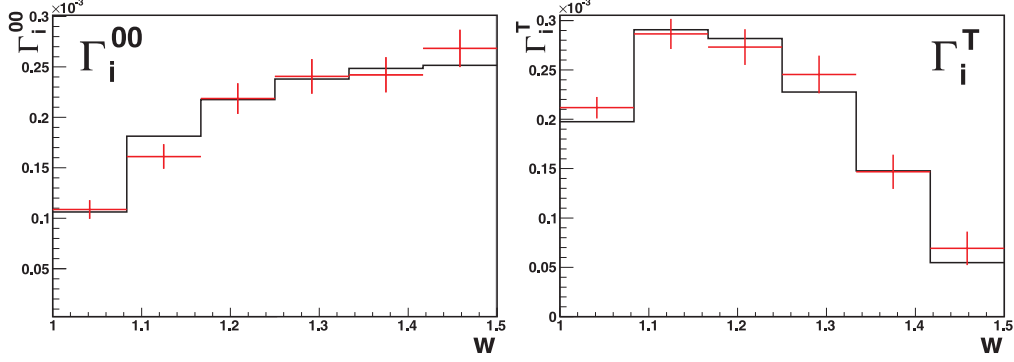


FIG. 11: Results of the fit of the helicity amplitudes (red crosses) compared to the prediction obtained by using the parametrization prescription by Caprini *et al.* [3] (solid black line). The left plot shows the results for Γ_i^{00} , the right one for Γ_i^T . Only the statistical error is shown.

B. Results

Given the very high amount of background in the $D^0 \rightarrow K^-\pi^+\pi^-\pi^+$ mode, we use only the $K\pi, e$ and $K\pi, \mu$ channels to determine the partial decay widths for each of the helicity components. Tables V and VI give the results of the fits, where the systematic errors quoted in these tables stem from the same sources as given in the breakdown in Table IV. It is dominated by the track reconstruction errors of the three charged tracks ℓ, π, K and the uncertainty of the π_s^0 reconstruction. The χ^2 of the fit is in good statistical agreement with the number of degrees of freedom, we obtain $\chi^2/\text{ndf} = 82.6/60$ or a χ^2 probability of $P_{\chi^2} = 2.8\%$. The results are shown in Fig. 11. There is good agreement with the results of the parametrized fit.

VI. SUMMARY AND DISCUSSION

We have reconstructed about 27,000 $B^+ \rightarrow \bar{D}^{*0}\ell^+\nu_\ell$ decays in the 140 fb^{-1} of Belle $\Upsilon(4S)$ data. A fit to the theoretical expression for the four-dimensional differential decay width (Eq. 10), assuming the parameterization of the helicity amplitude given by Caprini *et al.* [3] yields a measurement of $|V_{cb}|$ times the form factor normalization at zero recoil, $\mathcal{F}(1)|V_{cb}| = (35.0 \pm 0.4 \pm 2.2) \times 10^{-3}$. At the same time we determine the parameters of the Caprini *et al.* parameterization, $\rho^2 = 1.376 \pm 0.074 \pm 0.056$, $R_1(1) = 1.620 \pm 0.091 \pm 0.092$, $R_2(1) = 0.805 \pm 0.064 \pm 0.036$. The branching fraction of the decay $B^+ \rightarrow \bar{D}^{*0}\ell^+\nu_\ell$ is measured to be $(4.84 \pm 0.04 \pm 0.56)\%$. For all numbers quoted here, the first error is the statistical and the second is the systematic uncertainty. All results are preliminary. These measurements are in agreement with previous investigations of the decay $B^+ \rightarrow \bar{D}^{*0}\ell^+\nu_\ell$ [6, 7, 8].

A direct, model-independent determination of the form factor shapes has also been carried out and shows good agreement with the HQET based form factor parametrization by Caprini

	$D^0 \rightarrow K\pi, \ell = e$	$D^0 \rightarrow K\pi, \ell = \mu$
$\Gamma^T, w \in (1, \frac{13}{12})$	$(2.267 \pm 0.153 \pm 0.264) \times 10^{-4}$	$(1.939 \pm 0.152 \pm 0.228) \times 10^{-4}$
$\Gamma^T, w \in (\frac{13}{12}, \frac{7}{6})$	$(2.695 \pm 0.214 \pm 0.307) \times 10^{-4}$	$(3.015 \pm 0.216 \pm 0.348) \times 10^{-4}$
$\Gamma^T, w \in (\frac{7}{6}, \frac{15}{12})$	$(2.786 \pm 0.253 \pm 0.310) \times 10^{-4}$	$(2.678 \pm 0.261 \pm 0.299) \times 10^{-4}$
$\Gamma^T, w \in (\frac{15}{12}, \frac{8}{6})$	$(2.298 \pm 0.249 \pm 0.246) \times 10^{-4}$	$(2.673 \pm 0.295 \pm 0.290) \times 10^{-4}$
$\Gamma^T, w \in (\frac{8}{6}, \frac{17}{12})$	$(1.557 \pm 0.242 \pm 0.162) \times 10^{-4}$	$(1.369 \pm 0.250 \pm 0.144) \times 10^{-4}$
$\Gamma^T, w \in (\frac{17}{12}, 1.5)$	$(0.588 \pm 0.205 \pm 0.056) \times 10^{-4}$	$(0.862 \pm 0.284 \pm 0.099) \times 10^{-4}$
	fit to total sample	central value of parametrized fit
$\Gamma^T, w \in (1, \frac{13}{12})$	$(2.117 \pm 0.108 \pm 0.248) \times 10^{-4}$	1.975×10^{-4}
$\Gamma^T, w \in (\frac{13}{12}, \frac{7}{6})$	$(2.865 \pm 0.152 \pm 0.327) \times 10^{-4}$	2.908×10^{-4}
$\Gamma^T, w \in (\frac{7}{6}, \frac{15}{12})$	$(2.732 \pm 0.181 \pm 0.303) \times 10^{-4}$	2.819×10^{-4}
$\Gamma^T, w \in (\frac{15}{12}, \frac{8}{6})$	$(2.454 \pm 0.191 \pm 0.263) \times 10^{-4}$	2.276×10^{-4}
$\Gamma^T, w \in (\frac{8}{6}, \frac{17}{12})$	$(1.468 \pm 0.174 \pm 0.154) \times 10^{-4}$	1.478×10^{-4}
$\Gamma^T, w \in (\frac{17}{12}, 1.5)$	$(0.693 \pm 0.170 \pm 0.070) \times 10^{-4}$	0.547×10^{-4}

TABLE V: Obtained results for Γ_i^T , compared to the central values of the parametrized fit.

	$D^0 \rightarrow K\pi, \ell = e$	$D^0 \rightarrow K\pi, \ell = \mu$
$\Gamma^{00}, w \in (1, \frac{13}{12})$	$(1.025 \pm 0.119 \pm 0.120) \times 10^{-4}$	$(1.176 \pm 0.146 \pm 0.137) \times 10^{-4}$
$\Gamma^{00}, w \in (\frac{13}{12}, \frac{7}{6})$	$(1.544 \pm 0.165 \pm 0.176) \times 10^{-4}$	$(1.689 \pm 0.177 \pm 0.192) \times 10^{-4}$
$\Gamma^{00}, w \in (\frac{7}{6}, \frac{15}{12})$	$(2.238 \pm 0.213 \pm 0.237) \times 10^{-4}$	$(2.121 \pm 0.216 \pm 0.238) \times 10^{-4}$
$\Gamma^{00}, w \in (\frac{15}{12}, \frac{8}{6})$	$(2.677 \pm 0.244 \pm 0.268) \times 10^{-4}$	$(2.059 \pm 0.240 \pm 0.228) \times 10^{-4}$
$\Gamma^{00}, w \in (\frac{8}{6}, \frac{17}{12})$	$(2.406 \pm 0.235 \pm 0.256) \times 10^{-4}$	$(2.426 \pm 0.263 \pm 0.263) \times 10^{-4}$
$\Gamma^{00}, w \in (\frac{17}{12}, 1.5)$	$(2.907 \pm 0.250 \pm 0.301) \times 10^{-4}$	$(2.384 \pm 0.273 \pm 0.278) \times 10^{-4}$
	fit to total sample	central value of parametrized fit
$\Gamma^{00}, w \in (1, \frac{13}{12})$	$(1.087 \pm 0.092 \pm 0.123) \times 10^{-4}$	1.062×10^{-4}
$\Gamma^{00}, w \in (\frac{13}{12}, \frac{7}{6})$	$(1.611 \pm 0.121 \pm 0.179) \times 10^{-4}$	1.812×10^{-4}
$\Gamma^{00}, w \in (\frac{7}{6}, \frac{15}{12})$	$(2.186 \pm 0.151 \pm 0.238) \times 10^{-4}$	2.175×10^{-4}
$\Gamma^{00}, w \in (\frac{15}{12}, \frac{8}{6})$	$(2.406 \pm 0.172 \pm 0.262) \times 10^{-4}$	2.379×10^{-4}
$\Gamma^{00}, w \in (\frac{8}{6}, \frac{17}{12})$	$(2.421 \pm 0.175 \pm 0.258) \times 10^{-4}$	2.483×10^{-4}
$\Gamma^{00}, w \in (\frac{17}{12}, 1.5)$	$(2.683 \pm 0.186 \pm 0.298) \times 10^{-4}$	2.514×10^{-4}

TABLE VI: Obtained results for Γ_i^{00} , compared to the central values of the parametrized fit.

et al. [3].

- [1] M. Kobayashi and T. Maskawa, Prog. Theor. Phys. **49**, 652 (1973).
- [2] M. Neubert, Phys. Rept. **245**, 259 (1994) [arXiv:hep-ph/9306320].
- [3] I. Caprini, L. Lellouch and M. Neubert, Nucl. Phys. B **530**, 153 (1998) [arXiv:hep-ph/9712417].
- [4] C. Bernard *et al.*, Phys. Rev. D **79**, 014506 (2009) [arXiv:0808.2519 [hep-lat]].
- [5] E. Barberio *et al.* [Heavy Flavor Averaging Group], [arXiv:0808.1297 [hep-ex]].
- [6] H. Albrecht *et al.* [ARGUS Collaboration], Phys. Lett. B **275**, 195 (1992).
- [7] N. E. Adam *et al.* [CLEO collaboration], Phys. Rev. D **67**, 032001 (2003) [arXiv:hep-ex/0210040].
- [8] B. Aubert *et al.* [BABAR Collaboration], Phys. Rev. Lett **100**, 231803 (2008) [arXiv:0712.3493 [hep-ex]].
- [9] Throughout this note charge conjugation is implied.
- [10] C. Amsler *et al.* [Particle Data Group], Phys. Lett. B **667**, 1 (2008).
- [11] N. Isgur and M. B. Wise, Phys. Lett. B **232**, 113 (1989).
- [12] N. Isgur and M. B. Wise, Phys. Lett. B **237**, 527 (1990).
- [13] A. Abashian *et al.* [Belle Collaboration], Nucl. Instrum. Meth. A **479**, 117 (2002).
- [14] S. Kurokawa, Nucl. Instrum. Meth. A **499**, 1 (2003), and other papers included in this volume.
- [15] I. Adachi *et al.* [Belle Collaboration], [arXiv:0810.1657 [hep-ex]].
- [16] D. J. Lange, Nucl. Instrum. Meth. A **462**, 152 (2001).
- [17] R. Brun, F. Bruyant, M. Maire, A. C. McPherson and P. Zancarini, CERN-DD/EE/84-1.
- [18] E. Barberio and Z. Was, Comput. Phys. Commun. **79**, 291 (1994).
- [19] K. Abe *et al.* [Belle Collaboration], Phys. Rev. D **64**, 072001 (2001) [arXiv:hep-ex/0103041].
- [20] G. C. Fox and S. Wolfram, Phys. Rev. Lett. **41**, 1581 (1978).
- [21] K. Hanagaki, H. Kakuno, H. Ikeda, T. Iijima and T. Tsukamoto, Nucl. Instrum. Meth. A **485**, 490 (2002) [arXiv:hep-ex/0108044].
- [22] A. Abashian *et al.*, Nucl. Instrum. Meth. A **491**, 69 (2002).
- [23] Quantities evaluated in the c.m. frame are denoted by an asterisk.
- [24] R. J. Barlow and C. Beeston, Comput. Phys. Commun. **77**, 219 (1993).
- [25] R. Brun and F. Rademakers, Nucl. Instrum. Meth. A **389** (1997) 81.
- [26] F. James and M. Roos, Comput. Phys. Commun. **10**, 343 (1975).